PIV Measurement and CFD Computation for Sloshing Impact Flows

Kyung-Kyu Yang, Jieung Kim and Yonghwan Kim*
Department of Naval Architecture and Ocean Engineering, Seoul National University, Seoul, Korea
E-mail: *yhwankim@snu.ac.kr

1. Introduction

Violent sloshing problem is an important topic in the design of LNG related ships and offshore structures because sloshing flows can cause local impulsive pressure, providing potential danger of structural failure. Sloshing problems have been understood as stochastic phenomena. Therefore, a statistical analysis is essential to assess sloshing loads and numerous researches have been conducted to evaluate sloshing loads based on experimental methods. Conventional experiments, however, have technical and practical limitations. Pressure sensors are too large in their sizes in a model scale, and results are focused only on the pressure caused by the free surface without kinematic information of the fluids in a model tank.

In other way, many numerical studies on sloshing flows have been also reported in the past and being reported at present. Furthermore, there are myriad papers and applications by using various numerical methods. Conventional numerical methods provide similar results with experimental data in terms of global flow pattern even a coarse grid and simple modeling are used. However, prediction of impact pressure at the tank top of high filling cases is not yet accurate enough by using a conventional numerical method.

In the present study, sloshing model test with particle image velocimetry (PIV) measurement and the corresponding numerical computations solving incompressible flow are considered to compare the impact characteristics around the tank top corner. PIV measuring equipment (Ahn *et al*, 2012; Kim *et al*. 2014) which was synchronized with pressure measurement system at sloshing experimental facility in Seoul National University (SNU) is utilized in this study. The present numerical computation is based on both an in-house program of SNU and a commercial program, STAR-CCM+. In the case of the in-house program, a Cartesian-grid method (Yang *et al*. 2013) where the governing equation is solved by using a finite difference method and constraint-interpolation-profile (CIP) method.

The model test and numerical computation have been carried out for the scaled down benchmark test (Loysel *et al*. 2013). Among several test conditions, wet-drop type impact without trapped air is mainly concerned. Other complex physical phenomena such as compressibility, air pocket, vaporization, and condensation are not included. The comparison of the impact pressures and velocity fields between the numerical computation and experiment is made.

2. Experimental Setup for PIV Measurement

The main equipment in sloshing PIV experiment contains motion platform, model tank, high speed camera, laser, and pressure sensors as shown in Fig. 1(a). The motion platforms are hexapod type which consists of six actuators and the test model is a rectangular-shape tank with internal dimensions 630.7mm×446.7mm×78.7mm (L×H×B) as shown in Fig. 1(b). The reference frame is located at the center of tank bottom. x- and z-axes are pointing in longitudinal and vertical direction, respectively. High speed camera is required for capturing even small displacement of particles. The model of high speed camera is Y4-S2 from Integrated Design Tools (IDT) and its maximum capturing speed is about 4500 frame per second (FPS) for 1024×1024 pixel resolution. To illuminate PIV particles continuously, diode pumped solid state laser which can produce continuous wave is installed under the motion platform.

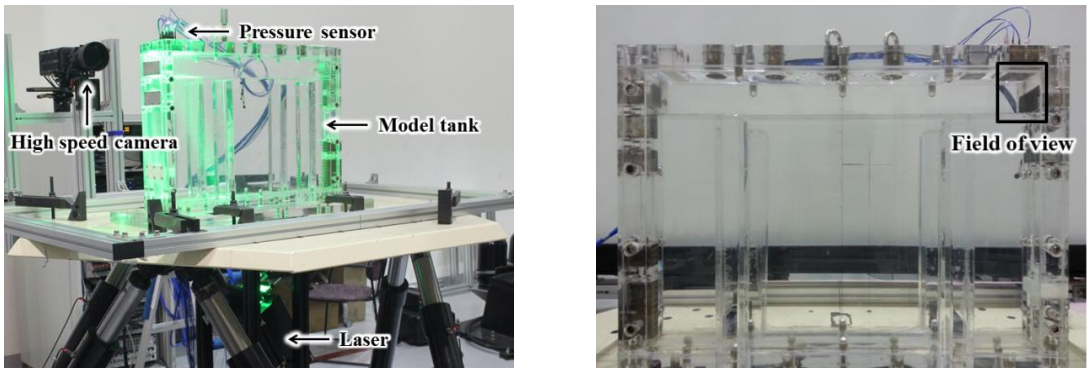

(a) Overview of PIV measurement system (b) Tank model and field of view

Fig. 1 Sloshing experiment set-up with PIV and pressure measurement system

Four dynamic pressure sensors which are numbered from the side wall as $P1$ to $P4$ are equipped around the right top corner. The type of pressure sensors is Integrated Circuit Piezoelectric (ICP) sensors made by KISTLER Co. The

sensors have a 5.54 mm sensing diameter and 20 kHz sampling rate is used in the present experiment. Pressure signals are obtained by Data Acquisition (DAQ) system which can handle over 20kHz of sampling rate and compatible with ICP sensors. The DAQ model is PXI-4495 board from National Instrument.

3. Numerical Method

3.1 Cartesian-Grid-Based Method

The present method is a CIP-based finite difference method on a Cartesian grid (Yang *et al.* 2014). Under the assumption of viscous and incompressible fluid, the governing equations to be considered for velocity $\vec{u}$ and pressure p are as follows:

$$\nabla \cdot \vec{u} = 0 \tag{1}$$

$$\frac{\partial \vec{u}}{\partial t} + \vec{u} \cdot \nabla \vec{u} = -\frac{1}{\rho}\nabla p + \frac{\mu}{\rho}\nabla^2 \vec{u} + \vec{f}_b \tag{2}$$

where ρ and μ are the density and dynamic viscosity of the fluid. The external force denoted by $\vec{f}_b$ includes the gravitational force, translational and rotational inertia forces.

Velocity and pressure are coupled by a fractional step method, involving a solving procedure that is divided into three steps, one advection and two non-advection phases. In the advection step, the equation with only advection terms is solved by using the CIP method. The external forces are considered in the first non-advection phase and the pressure field is then calculated through solving the pressure Poisson equation in the second non-advection phase. The other spatial discretization except advection terms is conducted based on the second-order central difference scheme.

The free-surface is determined by an interface capturing method. To identify the different phases in the multi-phase flow, density functions, ϕ_m, are defined for liquid (m=1) and gas (m=2). The density function for the liquid phase is calculated by using the tangent of hyperbola for interface capturing (THINC) scheme with the weighed line interface calculation (WLIC) method, which takes into account the information of the surface normal vector, while maintaining a simple implementation. The density function for the gas phase can then be calculated from a simple constraint that the summation of the density functions is equal to one for each cell.

3.2 Commercial Program

The commercial software, Star-CCM+ v9.06.011-R8, is also applied to simulate sloshing flow. In this simulation, the two-phase interactive free-surface ss simulated using VOF approach and Eulerian multiphase model. Two Eulerian phases, water and air, are inviscid and have constant densities. An implicit segregated method which fixes the time step during the time-marching process is chosen to solve the transport equations. Sloshing impact occurs in a very small localized area. Thus, to reduce the computation time, the concept of adaptive mesh model is applied for the present calculation. As shown in Fig. 2, a problem domain is divided into multiple zones, in which grid sizes are different. In the first zone, the grid size is defined as Δx. Meanwhile, grid sizes are enlarged to $2\Delta x$ and $4\Delta x$ in the second and third zone, respectively.

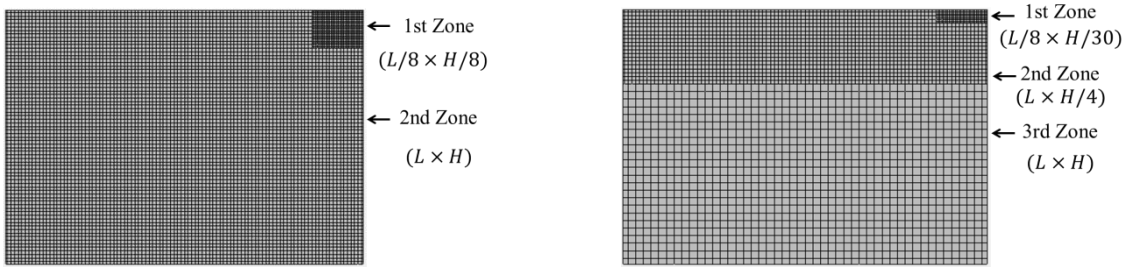

(a) Type 1 (b) Type 2

Fig. 2 Two types of adaptive mesh models

4. Experimental and Computational Results

To compare velocity field and pressure at the tank ceiling between the PIV measurement and CFD computation, a simple model problem is selected. The tank is excited by combination of a hyperbolic tangent and a sine function to generate an impact at the corner of tank top.

$$\theta(t)=\begin{cases}\theta_A \tanh\left(\pi\dfrac{t^2}{T}\right)\sin\left(2\pi\dfrac{t}{T}\right) & if\ t\le T\\ \theta_A \tanh\left(\pi\dfrac{(2T-t)^2}{T}\right)\sin\left(2\pi\dfrac{t}{T}\right) & if\ T<t\le 2T\end{cases} \tag{3}$$

Here, θ_A and T indicate roll amplitude and excitation period, respectively. Based on the previous benchmark study (Loysel *et al.* [3]**),** test condition is scaled down as θ_A=4.5° and ω/ω_n=1.075 (ω_n is the natural frequency of the fluid inside tank) with h/H=0.85 filling ratio. Rotational excitation along y-axis can generate a wet-drop type impact in which the free-surface hits the tank ceiling without trapped air.

4. Results and Discussion

The comparison of time histories of pressure obtained from the experiment and CFD computations is given in Fig. 3. In the computational results, the only finest grid (1600 × 1136 and $L/\Delta x_{\min}$ = 1600) case is shown. In the CIP-based method, two different pressure measuring methods – center pressure and spatially averaged pressure – are also compared. Compared to experimental data, the center pressure shows slightly overestimated peak value, while the spatially averaged pressure underestimates the peak pressure. The adaptive mesh computation shows similar peak value with the center pressure in the CIP-based method. In terms of overall pattern, however, is similar to each other except pressure at sensor "P1", which is located near the side wall. In the case of "P1" sensor, it shows the formation of air pocket around tank corner.

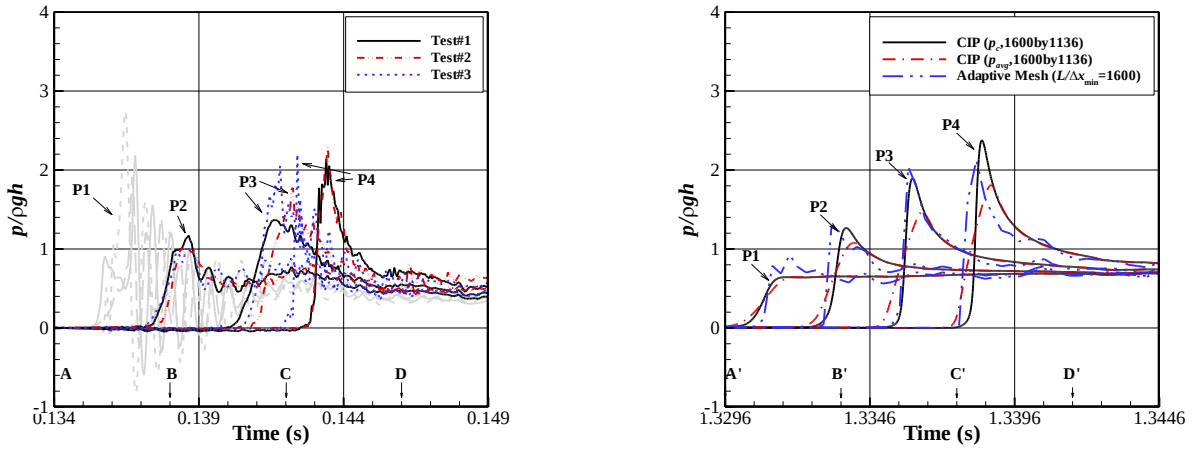

(a) Experiment (b) Computations

Fig. 3 Comparison of pressure time histories

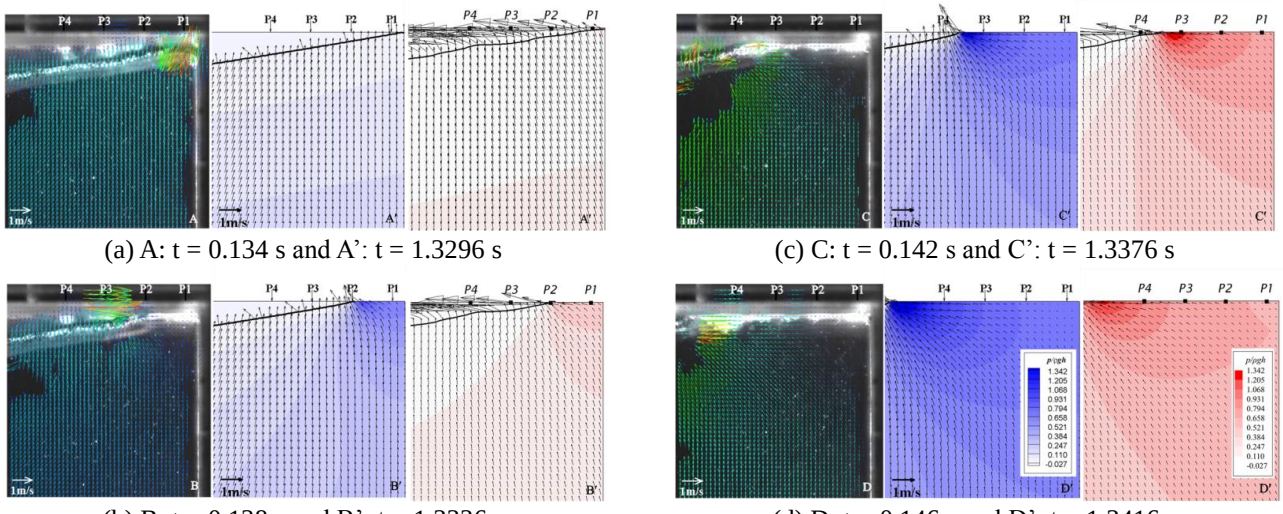

(a) A: t = 0.134 s and A': t = 1.3296 s (c) C: t = 0.142 s and C': t = 1.3376 s

(b) B: t = 0.138 s and B': t = 1.3336 s (d) D: t = 0.146 s and D': t = 1.3416 s

Fig. 4 Sequential snapshots of instantaneous free-surface shape and velocity vector for impact around top corner of the tank: PIV (left), CIP-based method (center), and adaptive mesh (right**)**

In Fig. 4, the sequential snapshots of the free-surface shape with the velocity vector show a comparison between the PIV measurement and CFD calculations. In the CFD results, the pressure distribution is also represented in contour map. The time increases from the top to bottom in 4-ms steps. The computational results show only the vertical direction velocity component before the free-surface hits the tank ceiling, as shown in Fig. 4(a). After the first impact occurs at the "P1" sensor location, the water moves to the left side, and a jet-flow is generated. The horizontal velocity increases with time, and the flow hits the pressure sensors in sequence. Similar patterns can be observed in the experimental results. However, trapped air and small air bubbles moved with the jet flow in experimental results, as previously discussed. In those regions, the laser light was scattered, and the image became white. In addition, the present model tank had a small hole (3-mm deep) in the front acrylic tank wall near the tank ceiling to prevent gas leakage in other experiment. Thus, it was difficult to obtain an accurate fluid velocity just below the tank ceiling in the present experiment.

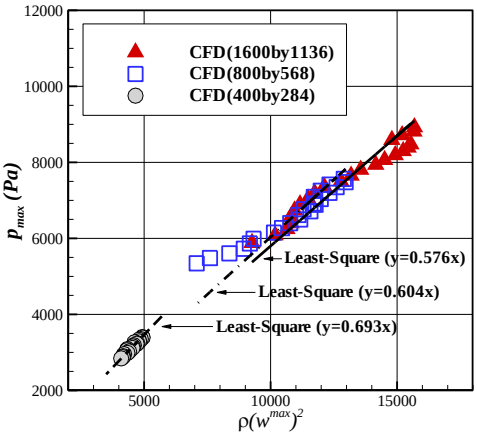

Fig. 5 Relationship between peak pressure and square of local maximum vertical velocity

When the impact pressure coefficient is calculated based on the maximum of local vertical velocity with the corresponding maximum pressure in each time, the impact pressure coefficient was about 0.58-0.6, which varied depending on the grid size, as shown in Fig. 5. Because the local vertical velocity increases as a jet flow is developed, the impact pressure coefficient based on the local flow is smaller than that based on the incidence flow. Even though the present result shows that the maximum pressure is proportional to the square of maximum velocity as is well known for a wet-drop case, further research is needed to obtain a universal relationship between the velocity and impact pressure to take into account more detailed flow physics of slosh-induced impact

5. Conclusions

Based on the present study, the following conclusions can be made:

- Overall pattern of flow motion can be obtained by PIV measurement. Except for the bubbly flow region, the current PIV measurement system provided results similar to the CIP-based computation.
- In the CIP-based numerical method, the impact pressure is quite sensitive to the grid resolution, while the time segment dependency affects weakly to the convergence of pressure peak. As the number of grid points increased, the peak pressure became larger, and the pressure reached a peak rapidly.
- For the adaptive mesh computation using commercial software, the impact pressure is sensitive to the refined grid size near the impact area and time-step size, while the type of refinement has a small influence to the impact pressure.
- The impact pressure coefficient from the CIP-based method is reasonable compared with a similarity solution. However, the relation between the impact pressure and local velocity is still not sufficiently clear. To obtain a deeper understanding of sloshing impact characteristics, systematic PIV experiments should be conducted and a computational code that considers the compressibility and hydro-elasticity should be developed.

Acknowledgements

This study has been supported by the LRF(Lloyd's Register Foundation)-Funded Research Center at Seoul National University for Fluid-Structure Interaction. Their support is greatly appreciated.

References

Ahn, Y, Kim, JH, Kim, SY, Kim, KH, and Kim, Y (2012). "Particle image velocimetry measurement on the oscillating characteristics of sloshing-induced internal flow fields," *Proc 6th Asis-Pacific Workshop on Marine Hydrodynamics*, Malaysia, 179-184.

Kim, J., Kim, J.-H., Kim, S.-Y., and Kim, Y., 2014. Measurement of Sloshing Flow using Particle Image Velocimetry. The 7th Asia-Pacific Workshop on Marine Hydrodynamics in Naval Architecture, Vladivostok, Russia.

Yang, K.-K., Kim, Y., Hu, C., 2010. Numerical Simulation of 2D Violent Sloshing Flows by Using CCUP Method. International Journal of Offshore and Polar Engineering, 20(3), 204-209.

Loysel, T., Gervaise, E., Moreau, S., and Brosset, L. 2013. Results of the 2012-2013 Sloshing Model Test Benchmark. The 23rd International Offshore and Polar Engineering Conference, ISOPE 2013, Alaska, USA.